Journal of Power Sources 196 (2011) 9924–9930

Contents lists available at SciVerse ScienceDirect

Journal of Power Sources

journal homepage: www.elsevier.com/locate/jpowsour

Studies of electrochemical performance of carbon supported Pt–Cu nanoparticles as anode catalysts for direct borohydride–hydrogen peroxide fuel cell

Lanhua Yi, Benan Hu, Yunfeng Song, Xianyou Wang*, Guishan Zou, Wei Yi

Key Laboratory of Environmentally Friendly Chemistry and Applications of Ministry of Education, School of Chemistry, Xiangtan University, Hunan 411105, PR China

ARTICLE INFO

Article history:
Received 23 July 2011
Accepted 13 August 2011
Available online 22 August 2011

Keywords:
Direct borohydride–hydrogen peroxide fuel cell
Anode electrocatalyst
Bimetallic catalyst
Borohydride oxidation
Catalytic activity

ABSTRACT

Carbon supported Pt–Cu bimetallic nanoparticles are prepared by a modified $NaBH_4$ reduction method in aqueous solution and used as the anode electrocatalyst of direct borohydride–hydrogen peroxide fuel cell (DBHFC). The physical and electrochemical properties of the as-prepared electrocatalysts are investigated by transmission electron microscopy (TEM), X-ray diffraction (XRD), cyclic voltammetry (CV), chronoamperometry (CA), chronopotentiometry (CP) and fuel cell test. The results show that the carbon supported Pt–Cu bimetallic catalysts have much higher catalytic activity for the direct oxidation of BH_4^- than the carbon supported pure nanosized Pt catalyst, especially the $Pt_{50}Cu_{50}$/C catalyst presents the highest catalytic activity among all as-prepared catalysts, and the DBHFC using $Pt_{50}Cu_{50}$/C as anode electrocatalyst and Pt/C as cathode electrocatalyst shows as high as 71.6 mW cm^{-2} power density at a discharge current density of 54.7 mA cm^{-2} at 25 °C.

1. Introduction

Fuels cells are actively investigated as an attractive alternative to conventional fossil fuel combustion engines for cleaner power generations [1,2]. Compared with a hydrogen combustion engine, a hydrogen fuel cell can directly change chemical energy into electrical energy with higher efficiency and requires gaseous hydrogen as fuel. However, there still remain some problems for transportation and storage of hydrogen. Direct borohydride–hydrogen peroxide fuel cell (DBHFC), especially using sodium borohydride ($NaBH_4$) aqueous solution as fuel, has been intensively studied [3–6]. Sodium borohydride ($NaBH_4$) contains high hydrogen content (weight content of 10.6%) and a high capacity (5.7 Ah g^{-1}). Moreover, sodium borohydride is non-toxic, rather safe, chemically stable, easy to store and transport in its dry state. Thus, sodium borohydride has been considered to be an attractive hydrogen source for DBHFCs.

The anode reaction of DBHFC in an aqueous alkaline medium according to an eight-electron mechanism is described as follows [7]:

$$BH_4^- + 8OH^- \rightarrow BO_2^- + 6H_2O + 8e^-, \quad E^0 = -1.24\,\text{Vvs.SHE} \qquad (1)$$

With the oxidation of $NaBH_4$ at the anode, the hydrogen peroxide in an acid electrolyte instead of oxygen as an oxidant can yield higher cell potential and energy density:

$$H_2O_2 + 2H^+ + 2e^- \rightarrow 2H_2O, \quad E^0 = 1.77\,\text{Vvs.SHE} \qquad (2)$$

In combination with the reduction of hydrogen peroxide, DBHFC can give a theoretical cell voltage of 3.01 V and presents a high energy density. Overall cell reaction is as follows:

$$BH_4^- + 4H_2O_2 \rightarrow BO_2^- + 6H_2O, \quad E^0_{cell} = 3.01\,\text{V} \qquad (3)$$

The anode electrocatalyst is one of the key components in fuel cell. In the past years, different metals have been studied as the anode electrocatalyst for DBHFC, such as Pt [8–10], Au [9–11], Os [12,13], Pd [14], Ag [15], Ni [16], Zn [17] and hydrogen storage alloys [18]. Among these metals, Pt, Au and Os are more attractive than other metals as anode catalyst for DBHFC. However, although it has been reported that the electrooxidation of BH_4^- on Au particles is an approximate eight-electron process [9,11], Chatenet et al. [19,20] recently find that Au does in fact show catalytic activity for hydrolysis of borohydride to some extent. Moreover, slow electrode kinetics of BH_4^- on Au anode results in low current and power output, and thus degrades the electrochemical performance of the DBHFC [21–23]. Gyenge et al. [12,13] investigated the DBFC using carbon supported Os and Os–alloys (Os–Sn, Os–Mo and Os–V) as anode catalysts, and found that Os could be a promising electrocatalyst for BH_4^- oxidation, but Os–alloys were not a good candidate due to their high positive overpotentials [13].

* Corresponding author. Tel.: +86 731 5829060; fax: +86 731 58292061.
E-mail address: wxianyou@yahoo.com (X. Wang).

0378-7753/$ – see front matter © 2011 Elsevier B.V. All rights reserved.
doi:10.1016/j.jpowsour.2011.08.063

Up to now, platinum has been intensively studied on anode electrocatalyst of DBFC [8–10,24], but Pt is a noble metal and will result in a high cost. Many efforts have been made to lower the cost of catalyst; one way is to alloy Pt with transition metals such as Co [25], Ni [26], Sn [27], Fe [28] and Cr [29]. It has been reported that the Pt-based alloys have demonstrated similar or even higher electrocatalytic activities than the simplex Pt catalyst [25–29]. Wang et al. [30] investigated Pt–Ni/C as anode electrocatalyst for the DBFC, and found that the addition of Ni to Pt/C results in the improvement of the electrocatalytic activity. Gyenge et al. [31] studied the DBFC using carbon supported Pt and Pt–alloys (Pt–Ir/C, Pt–Ni/C, and Pt–Au/C) as anode catalyst, and found that Pt–Ir/C and Pt–Ni/C gave the higher cell voltage at a given superficial current density than Pt/C and Pt–Au/C. However, Cu is relatively inexpensive metal, to the best of our knowledge, Pt–Cu bimetallic nanoparticles supported on carbon as anodic catalyst for BH_4^- electro-oxidation were barely studied. In this work, a series of Pt–Cu bimetallic nanoparticles supported on carbon black XC-72R (Pt–Cu/C) were prepared by a modified $NaBH_4$ reduction method in aqueous solution and used as the anode catalyst for BH_4^- electro-oxidation. The electrochemical evaluations of catalytic activity for the as-prepared catalysts were carried out by cyclic voltammetry (CV) chronoamperometry (CA) and chronopotentiometry (CP). Moreover, the performances of the DBHFC employing Pt–Cu/C as the anode catalyst and Pt/C as the cathode catalyst were studied in detail.

2. Experimental methods

All chemical reagents were of analytical grade: sodium borohydride (AlfaAesar, 98%), hexachloroplatinicacid (Sigma–Aldrich), cupric sulfate (Sigma–Aldrich), polyvinylpyrrolidone (Sigma–Aldrich), Vulcan XC-72R carbon (Cabot Corp., 240 $m^2\ g^{-1}$) and Nafion solution (Dupont, 5%).

2.1. Preparation of Pt–Cu/C catalysts

$HPtCl_6{\cdot}5H_2O$ and $CuSO_4{\cdot}5H_2O$ were used as precursors of Pt–Cu bimetallic catalysts. XC-72R carbon black and $NaBH_4$ were used as a support and reducing agent, respectively. Polyvinylpyrrolidone (PVP) was used to prevent nanoparticles from aggregating in the solution. A brief description of the preparation method is as follows: the required amounts of $HPtCl_6$, $CuSO_4$, carbon and PVP were added to 100 ml deionized (DI) water under vigorous stirring, and then it was kept to stir for 30 min. The pH of the mixed solution was adjusted to 10 by adding 3 M NaOH solution, and 1 ml of 1 M $NaBH_4$ was added dropwise. After an additional 24 h stirring, the resulting catalyst was filtered and washed with deionized water until no Cl^- was detected, finally dried for 12 h at 80 °C in vacuum to obtain Pt–Cu/C catalysts. The atomic ratios of Pt/Cu which contained in the impregnation solutions were 100:0, 67:33, 50:50 and 33:67. The prepared four catalysts were denoted as Pt/C, $Pt_{67}Cu_{33}$/C, $Pt_{50}Cu_{50}$/C and $Pt_{33}Cu_{67}$/C, respectively. For each catalyst, the amount of metal is 20 wt.% of total catalyst weight.

2.2. Physical characterization of Pt–Cu/C electrocatalysts

The structure and morphology of the prepared electrocatalyst were examined by transmission electron microscopy (TEM), using a Jeol 3010 microscope at 300 kV. For TEM analyses, samples were prepared by placing one or two drops of nanoparticles solution onto the carbon-coated copper grid and drying it in air at room temperature.

X-ray diffractometer (D/MAX-3C) was employed with Cu Kα radiation (λ = 1.54056 Å) and a graphite monochromator at 50 kV, 100 mA to obtain X-ray diffraction (XRD) patterns of the samples. The 2θ angular regions between 10° and 80° were explored at a scan rate of 5° min^{-1}.

2.3. Electrochemical performance of anode catalysts

Electrochemical measurements were performed using CHI660A Electrochemistry Workstation and a typical three-electrode one-compartment electrolysis cell. The Pt–Cu/C or Pt/C was used as working electrode, a Ni foam mesh with 3 cm × 5 cm as counter electrode and an Ag/AgCl, KCl_{std} as the reference electrode. The electrolyte was 0.1 M $NaBH_4$ + 3.0 M NaOH. The working electrode was prepared as follows: 10 mg of Pt–Cu/C or Pt/C powder was dispersed by ultrasonic for 2 h in 1 ml blend solution of 0.25 ml 5 wt.% Nafion solution and 0.75 ml de-ionized water. Then 5 μl of slurry was pasted on the surface of the glassy carbon (GC) electrode (3 mm in diameter) which was polished to mirror by 0.5 μm alumina and sonicated 5 min prior to use. The dispersed catalyst on the GC surface was dried for 5 h at room temperature. The loading mass of catalyst was 0.7 mg cm^{-2} and actual metal loading mass on electrode is 0.14 mg cm^{-2}.

2.4. Fuel cell test

The catalyst ink was made by mixing isopropyl alcohol with 7 wt.% of Nafion solution and carbon supported catalysts. Then the ink was coated onto a stainless steel gauze resulting in a 4.5 mg cm^{-2} catalyst loading, and actual metal loading mass on electrode is 0.9 mg cm^{-2}. The catalyst electrodes were pressed at 10 MPa for 1 min to ensure a good electric contact, then dried at 50 °C for 8 h in vacuum.

The cell performance was tested against a Pt/C cathode and a Pt–Cu/C or Pt/C anode. A schematic diagram of the experimental set-up was shown in our previous studies [32]. A Nafion 117 membrane was used to separate the anolyte and catholyte. Anolyte is composed of 1 M $NaBH_4$ + 3 M NaOH, and the catholyte is composed of 2 M H_2O_2 + 0.5 M H_2SO_4. The fresh anolyte and catholyte were continuously supplied and withdrawn from the cell at a rate of 0.7 ml min^{-1}, respectively. The load was applied in steps of 5 mA within the range of 0–90 mA. Each step lasted 2 min and the current was continuously applied from one value to next without disconnecting the cell. The cell testing was performed using a battery testing system (Xinwei, Shenzhen, China). Power densities were calculated from the applied current and steady state potential.

3. Results and discussion

3.1. Physical characterization

Fig. 1(a) and (b) is the TEM and HR-TEM images of the $Pt_{50}Cu_{50}$/C catalysts. It can be clearly seen that the metal nanoparticles with a narrow particle size distribution are uniformly dispersed on the surface of carbon. The morphologies of the metal nanoparticles are generally spherical, and the mean diameter is approximately 3 nm. Fig. 2 shows the XRD patterns of the Pt/C, $Pt_{67}Cu_{33}$/C, $Pt_{50}Cu_{50}$/C and $Pt_{33}Cu_{67}$/C. The wide diffraction peak located at a 2θ value of about 25.0° is attributed to carbon (0 0 2) crystal face, which matches well with the standard C peak (JCPDS No. 75-1621). The diffraction peaks positioned at 2θ = 39°, 46°, 67° could be indexed to the (1 1 1), (2 0 0), (2 2 0) planes of face-centered cubic (fcc) Pt, which match well with the standard Pt peaks (JCPDS No. 88-2343). The diffraction peaks positioned at 2θ = 35.4° and 38.7° on the XRD pattern of $Pt_{33}Cu_{67}$/C are attributed to (0 0 2) and (1 1 1) planes of end-centered monoclinic CuO, which match well with the standard CuO peaks (JCPDS No. 80-1917). However, no diffraction peaks of Cu or its oxides are observed for $Pt_{67}Cu_{33}$/C and $Pt_{50}Cu_{50}$/C, indicating that Pt metal and Cu metal are alloyed well. And the XRD

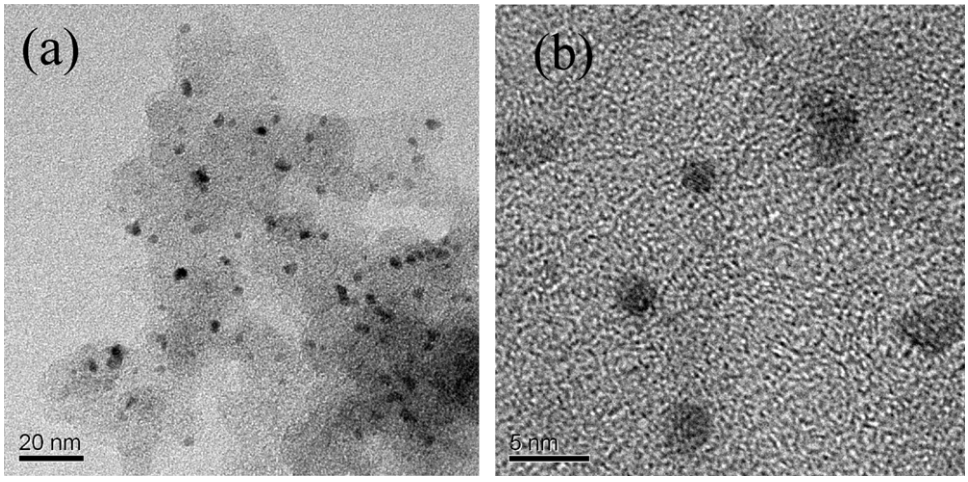

Fig. 1. TEM (a) and HR-TEM (b) images of $Pt_{50}Cu_{50}$ nanoparticles dispersed on carbon.

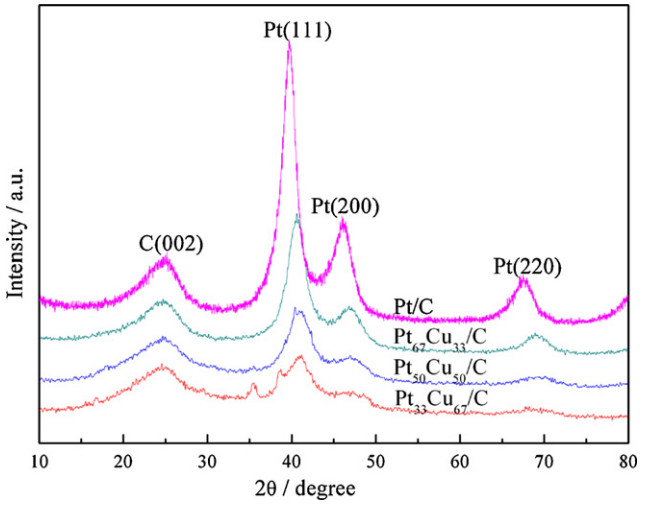

Fig. 2. XRD patterns of Pt–Cu/C with different proportion of Cu dispersed on carbon.

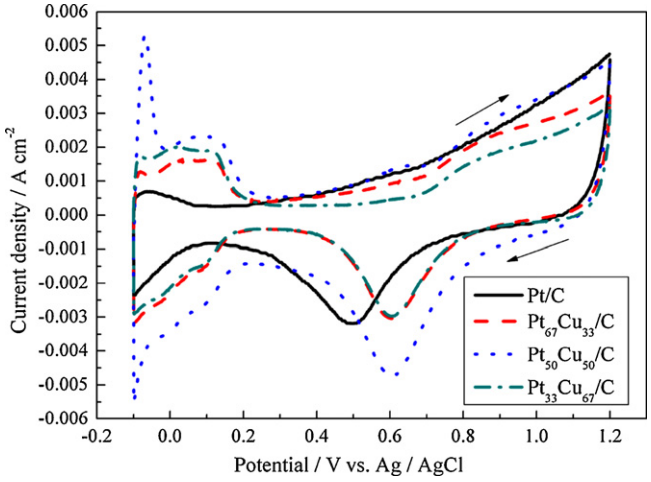

Fig. 3. Cyclic voltammograms of Pt/C and Pt–Cu/C electrodes in Ar-saturated 0.5 M H_2SO_4 solution at a scan rate of 50 mV s^{-1}.

pattern of $Pt_{33}Cu_{67}$/C with high Cu content appears CuO diffraction peaks, the reasons are probably because Pt atom and Cu atom are only partially alloyed, and the residual Cu atom is oxidized.

The diffraction peak for Pt (2 0 0) is used to estimate the particle size by the Scherrer's equation [26,33]:

$$D = \frac{0.9\lambda}{B\cos\theta} \quad (4)$$

where D is average particle size, nm, the wavelength λ is equal to 0.154056 nm, θ is the angle of Pt (2 0 0) peak and B is the full width at half-maximum in radians (FWHM). The calculated average particle size of $Pt_{50}Cu_{50}$ nanoparticles dispersed on carbon is about 3.2 nm, which is well consistent with the TEM results.

3.2. Electrochemically active surface area estimation

Electrochemically active surface area (ECSA) of the electrocatalysts could be estimated from the coulombic charge for the hydrogen adsorption and desorption (Q_H) in the cyclic voltammograms [34]. Cyclic voltammograms were recorded from −0.1 V to 1.2 V at a scan rate of 50 mV s^{-1} in a 0.5 M H_2SO_4 solution, high purity argon gas was used during the experiments and argon gas

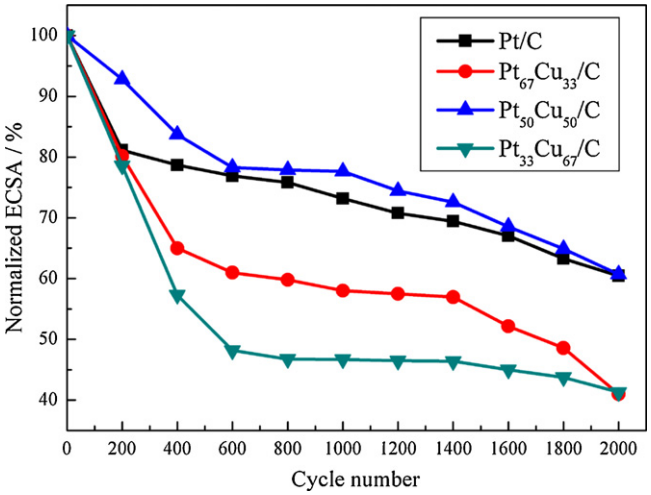

Fig. 4. Changes of electrochemical active surface area of Pt/C and Pt–Cu/C electrodes with different cycle number.

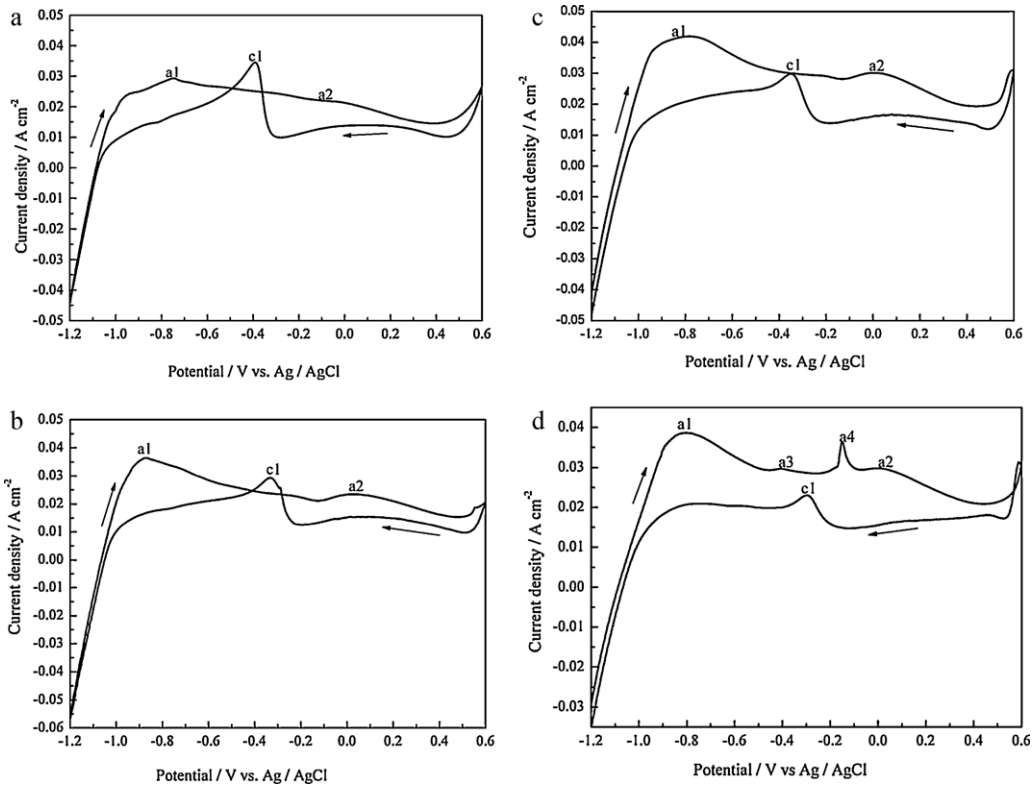

Fig. 5. Cyclic voltammograms in 0.1 M $NaBH_4$ + 3.0 M NaOH at a potential scan rate of 20 mV s^{-1} at anode catalysts. (a) Pt/C, (b) $Pt_{67}Cu_{33}$/C, (c) $Pt_{50}Cu_{50}$/C, (d) $Pt_{33}Cu_{67}$/C.

was bubbled for 30 min to eliminate oxygen prior to experiment (Fig. 3). ECSA can be calculated based on Eq. (5) [34,35].

$$\mathrm{ECSA} = \frac{Q_H}{[\mathrm{Pt}] \times 0.21} \tag{5}$$

where Q_H is calculated as the mean value between the amounts of charge transfer during the electro-adsorption and desorption of H_2 on Pt sites, mC cm^{-2}, 0.21 is the charge required to oxidize a monolayer hydrogen adsorption on bright Pt [36], mC cm^{-2}, and [Pt] is the platinum loading in the electrode, mg cm^{-2}. The calculated ECSAs of the Pt/C, $Pt_{67}Cu_{33}$/C, $Pt_{50}Cu_{50}$/C and $Pt_{33}Cu_{67}$/C are 128.6 cm^2 mg^{-1}, 224.5 cm^2 mg^{-1}, 340.3 cm^2 mg^{-1}, and 269.1 cm^2 mg^{-1}, respectively. And among the four electrocatalysts, $Pt_{50}Cu_{50}$/C has the highest ECSA, which is attributed to the small particle size of Pt nanoparticles loaded on the carbon [37].

The stabilities of Pt/C, $Pt_{67}Cu_{33}$/C, $Pt_{50}Cu_{50}$/C and $Pt_{33}Cu_{67}$/C were investigated by repeatedly cyclic voltammetry measurement in the potential range of −0.1 V to 1.2 V in 0.5 M H_2SO_4 solution [37,38]. Then, the ECSA for given catalyst in each cycle was calculated, and the stability of catalyst was compared based on the change of ECSA. Fig. 4 shows the changes of ECSA with the increasing cycle numbers. As seen in Fig. 4, the ECSAs of all electrocatalysts are decreased after the 2000 cycles, but Pt/C, $Pt_{67}Cu_{33}$/C, $Pt_{50}Cu_{50}$/C and $Pt_{33}Cu_{67}$/C retains 60.43%, 40.99%, 60.71%, and 40.30% of the initial ECSA, respectively. The above results indicate apparently that all electrocatalysts have good long-term running stability, especially $Pt_{50}Cu_{50}$/C presents the same good stability as Pt/C.

3.3. Cyclic voltammetry

The cyclic voltammetries recorded for Pt/C, $Pt_{67}Cu_{33}$/C, $Pt_{50}Cu_{50}$/C and $Pt_{33}Cu_{67}$/C electrodes with 0.1 M $NaBH_4$ + 3.0 M NaOH solution at a scan rate of 20 mV s^{-1} in the potential range of −1.2 V to 0.6 V vs. Ag/AgCl, KCl_{std} are shown in Fig. 5. The Pt–Cu/C and Pt/C electrodes show a similar catalytic behavior for the electrooxidation of BH_4^- by comparing the shapes of all CV curves between −1.2 and 0.6 V vs. Ag/AgCl. According to the CV curves, the electrochemical behavior of BH_4^- is complicated for a number of oxidation peaks. During the forward sweep, a well-defined oxidation peak (a1) occurs at about −0.8 V, followed by a broad hump anodic peak (a2). And with the increasing content of Cu, another two anodic peaks (a3 and a4) were observed for $Pt_{33}Cu_{67}$/C electrode. During the reverse sweep, a sharp anodic spike (c1) is observed. Similar anodic–cathodic peak patterns in cyclic voltammetry have reported by Gyenge [9] and Concha and Chatenet [39]. The first anodic peak (a1) can be assigned to borohydride hydrolysis followed by the electrooxidation of H_2, the second oxidation peak (a2) is attributed to the direct oxidation of BH_4^- in absence of H_2 electroxidation, and the peak (c1) is due to the oxidation of absorbed intermediate oxidation products of BH_3OH^- (Eq. (7)) on the partially oxidized Pt surface [9,39].

$$BH_4^- + H_2O \rightarrow BH_3OH^- + H_2 \tag{6}$$

$$BH_3OH^- + 3OH^- \rightarrow BO_2^- + \tfrac{3}{2}H_2 + 2H_2O + 3e^- \tag{7}$$

In addition, for the CV curve of $Pt_{33}Cu_{67}$/C electrode (Fig. 5(d)), the anodic peak a3 manifests Cu_2O formation, while the anodic peaks a4 represents formation of CuO and $Cu(OH)_2$ [40].

For direct oxidation of BH_4^-, the anodic current densities of peak a2 on Pt/C, $Pt_{67}Cu_{33}$/C, $Pt_{50}Cu_{50}$/C, and $Pt_{33}Cu_{67}$/C are 21.88, 23.43, 30.13, and 29.77 mA cm^{-2}, respectively. Although the content of Pt in Pt–Cu/C catalysts is less than that in Pt/C, the peak current densities on the serial Pt–Cu/C electrodes are hardly reduced. On the contrary, all the peak current densities for a2 on Pt–Cu/C electrodes are higher than that on Pt/C electrode. It can be attributed to the synergistic effect of Pt–Cu bimetallic nanoparticles, which jointly improves the electrochemical oxidation of BH_4^- [32]. Among the four electrocatalysts, the peak current density of a2 on the $Pt_{50}Cu_{50}$/C is the highest, thus the $Pt_{50}Cu_{50}$/C catalyst will show the highest catalytic activity for the electrooxidation of BH_4^-.

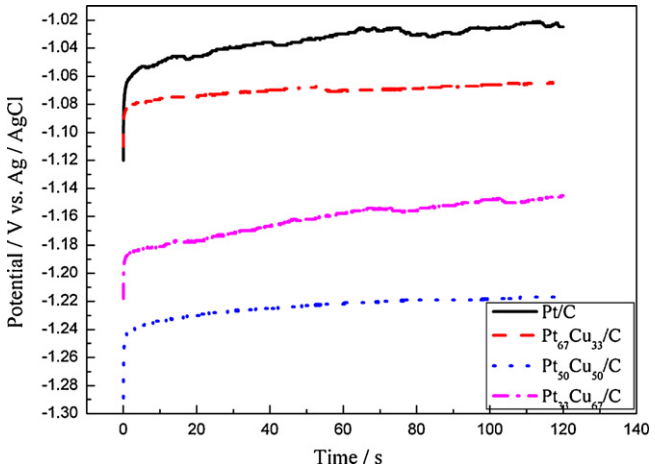

Fig. 6. Chronopotentiometry curves of Pt/C and Pt–Cu/C electrodes in 0.1 M $NaBH_4$ + 3.0 M NaOH solution. Current step: from 0 to 8.5 mA cm^{-2}.

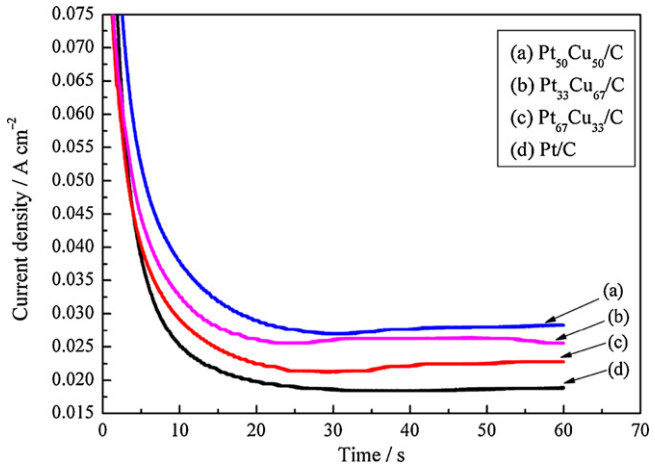

Fig. 7. Chronoamperometry curves of Pt/C and Pt–Cu/C electrodes in 0.1 M $NaBH_4$ + 3.0 M NaOH solution. Potential step: from −1.2 to −0.2 V vs. Ag/AgCl.

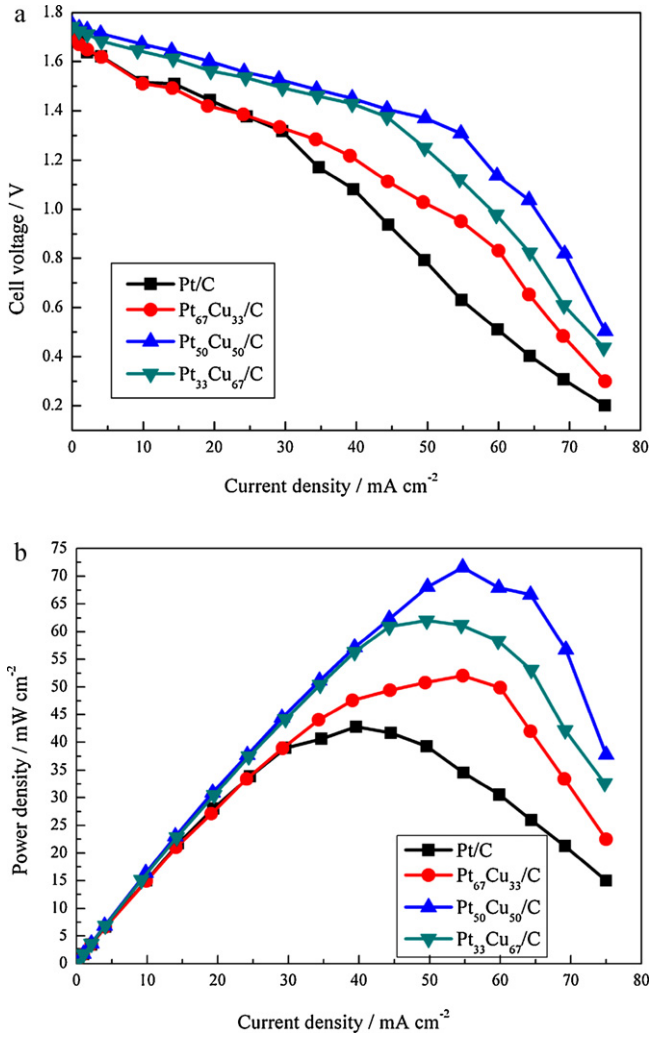

Fig. 8. Cell polarization curves (a) and power density curves (b) of the DBHFC using different anode catalysts at 25 °C with 1 M $NaBH_4$ + 3 M NaOH anolyte and 2 M H_2O_2 + 0.5 M H_2SO_4 catholyte. Catalyst loading: 4.5 mg cm^{-2}.

3.4. Chronopotentiometry

Being analogy with the constant current operation of a direct borohydride fuel cell, chronopotentiometry could provide further information about electrocatalytic activity of BH_4^- electrooxidation process on the different electrodes [41]. Fig. 6 compares the chronopotentiograms of Pt/C, $Pt_{67}Cu_{33}$/C, $Pt_{50}Cu_{50}$/C, and $Pt_{33}Cu_{67}$/C electrodes at a current density of 8.5 mA cm^{-2} in 0.1 M $NaBH_4$ + 3.0 M NaOH solution. It is well known that a lower overpotential is an indication of better electrocatalytic activity. As shown in Fig. 6, it can be clearly seen that $Pt_{50}Cu_{50}$/C exhibits the smallest overpotential (about −1.217 V). The order of overpotential of four electrodes is $Pt_{50}Cu_{50}$/C < $Pt_{33}Cu_{67}$/C < $Pt_{67}Cu_{33}$/C < Pt/C, thus $Pt_{50}Cu_{50}$/C will exhibit highest direct electrooxidation catalytic activity and power output among all catalysts.

3.5. Chronoamperometry

Chronoamperometric technique is another effective method to evaluate the electrocatalytic activity of catalyst. Fig. 7 shows the chronoamperometric responses of Pt/C, $Pt_{67}Cu_{33}$/C, $Pt_{50}Cu_{50}$/C and $Pt_{33}Cu_{67}$/C electrodes in 0.1 M $NaBH_4$ + 3.0 M NaOH solution from −1.2 to −0.2 V vs. Ag/AgCl, KCl_{std}. It can be observed from Fig. 7 that all four samples show an initial current decay during the electrooxidation process of BH_4^-. After 60 s, the Pt–Cu/C electrodes deliver higher current density than the Pt/C electrode. The current densities for Pt/C, $Pt_{67}Cu_{33}$/C, $Pt_{50}Cu_{50}$/C and $Pt_{33}Cu_{67}$/C are 18.83 mA cm^{-2}, 22.79 mA cm^{-2}, 28.31 mA cm^{-2} and 25.58 mA cm^{-2}, respectively. Apparently, the sequence of catalytic activity of four electrodes is $Pt_{50}Cu_{50}$/C > $Pt_{33}Cu_{67}$/C > $Pt_{67}Cu_{33}$/C > Pt/C, therefore, it is further demonstrated that $Pt_{50}Cu_{50}$/C catalyst exhibits the best catalytic performance among the all four electrodes, and it can be expected that the DBHFC with $Pt_{50}Cu_{50}$/C anode catalyst will show the highest power output.

3.6. Fuel cell performance measurement

Fig. 8 shows the changes of cell voltage and power density of DBHFCs with current density at 25 °C using Pt/C, $Pt_{67}Cu_{33}$/C, $Pt_{50}Cu_{50}$/C and $Pt_{33}Cu_{67}$/C as anode catalysts. The cathode catalyst of all DBHFCs systems was Pt/C. The anolyte was 3 M NaOH + 1 M $NaBH_4$ solution, and the catholyte was 0.5 M H_2SO_4 + 2 M H_2O_2 solution according to our previous studies [32]. The open circuit voltage (OCV) of the cell is about 1.7 V, which is lower than the standard cell potential for the DBHFC in acid electrolyte. The low value is probably caused by mixed potential at the anode and cathode from simultaneous oxidation of BH_4^- ions and hydrogen at the anode and reduction of H_2O_2 and O_2 at the cathode [42]. The change of the cell voltage vs. current density obtained using Pt–Cu/C as

Table 1
The comparison of DBFC performances using different anode electrocatalysts.

Anode electrocatalyst	Cathode electrocatalyst	Membrane	Fuel	Oxidation	Power density ($mW\,cm^{-2}$)	T (°C)	Mass activity basis ($W\,g^{-1}$ anode catalyst)	Ref.
Au/C (0.5 mg Au cm^{-2})	Pt/C (4 mg Pt cm^{-2})	Nafion 117	25% $NaBH_4$ + 6 M NaOH	1 M H_2O_2 + 1 M HCl + 3 M NaCl	34	20	68	[5]
$Au_{58}Ni_{42}$/C (0.9 mg metal cm^{-2})	Au/C (0.9 mg Pt cm^{-2})	Nafion 117	1 M $NaBH_4$ + 3 M NaOH	2 M H_2O_2 + 0.5 M H_2SO_4	45.7	20	50.8	[32]
Os/C (1 mg Os cm^{-2})	Pt black (4 mg Pt cm^{-2})	Nafion 117	0.5 M $NaBH_4$ + 2 M NaOH	O_2: Flowrate: 1.25 l min^{-1}	18	25	18	[12]
Pt–Ni/C(mole, 1:1) (5 mg metal cm^{-2})	Pt/C (4 mg Pt cm^{-2})	Nafion 117	2 M $NaBH_4$ + 2 M NaOH	O_2: Flowrate: 0.2 l min^{-1}	69	60	69	[31]
Pt/C (0.9 mg Pt cm^{-2})	Pt/C (0.9 mg Pt cm^{-2})	Nafion 117	1 M $NaBH_4$ + 3 M NaOH	2 M H_2O_2 + 0.5 M H_2SO_4	42.8	25	47.6	
$Pt_{50}Cu_{50}$/C (0.9 mg metal cm^{-2})	Pt/C (0.9 mg Pt cm^{-2})	Nafion 117	1 M $NaBH_4$ + 3 M NaOH	2 M H_2O_2 + 0.5 M H_2SO_4	71.6	25	79.6	

anode catalysts shows similar linear behavior as Pt/C anode catalysts, however, the cell voltage dropped more slowly as the current density increased. And the fuel cell using $Pt_{50}Cu_{50}$/C as anode catalyst gives the best performance and the maximum power density is 71.6 mW cm^{-2} at a current density of 54.7 mA cm^{-2} at 25 °C, which is much higher than that of using Pt/C (42.8 mW cm^{-2}). Though the loading amount of Pt in Pt–Cu/C is clearly less than that in Pt/C, the DBHFC using Pt–Cu/C as anode catalysts shows still significantly better performance than Pt/C as the anode catalysts.

Table 1 tabulated the comparison of DBFC performances using different anode electrocatalysts, such as Au/C, Au–Ni/C, Os/C, Pt–Ni/C, Pt/C and $Pt_{50}Cu_{50}$/C. Apparently, although substitution of 50% Cu for Pt will result in a large decrease of the catalyst cost, $Pt_{50}Cu_{50}$/C still reveals parallel or even much higher catalytic activity toward BH_4^- oxidation. Therefore, $Pt_{50}Cu_{50}$/C will be a promising catalyst to make less expensive fuel cell.

4. Conclusions

(1) Carbon-supported Pt and Pt–Cu bimetallics nanoparticles for the DBHFC anode catalysts were prepared by a modified $NaBH_4$ reduction method in aqueous solution. The Pt–Cu alloy nanoparticles with a narrow particle size distribution are uniformly dispersed on the surface of carbon support, and the average size of the Pt–Cu alloy nanoparticles was about 3.2 nm.
(2) The Pt–Cu/C electrodes show the same catalytic behavior as Pt/C electrode for the electrooxidation of BH_4^-. Although the serial Pt–Cu alloy catalysts show a relatively low cost, they represent much higher electrochemical catalytic activity for BH_4^- oxidation than Pt/C in the alkaline solution, especially the $Pt_{50}Cu_{50}$/C reveals the highest electrocatalytic activity to the direct oxidation of BH_4^-.
(3) The serial Pt–Cu alloy catalysts have good long-term running stability; especially $Pt_{50}Cu_{50}$/C reveals the same good stability as Pt/C. The sequence of catalytic activity of serial Pt–Cu alloy catalysts is $Pt_{50}Cu_{50}$/C > $Pt_{33}Cu_{67}$/C > $Pt_{67}Cu_{33}$/C > Pt/C.
(4) The DBHFCs using Pt–Cu/C as the anode catalyst exhibits excellent electrochemical performance compared with Pt/C as the anode catalyst, and the maximum power density of the DBHFC employing $Pt_{50}Cu_{50}$/C as the anode catalyst and Pt/C as the cathode catalyst was 71.6 mW cm^{-2} at 25 °C.

Therefore, the carbon supported Pt–Cu bimetallic catalysts with high performance and low cost will be a promising anode catalyst for the application of DBHFCs.

Acknowledgments

This work was financially supported by the National Natural Science Foundation of China (Grant Nos. 20871101 and 51072173), Doctoral Fund of Ministry of Education of China (Grant No. 20094301110005), the Science and Technology Plan Project of Hunan Province (Grant No. 2010GK3181).

References

[1] M. Miller, A. Bazylak, J. Power Sources 196 (2011) 601–613.
[2] B.C.H. Steele, A. Heinzel, Nature 414 (2001) 345–352.
[3] D.X. Cao, D.D. Chen, J. Lan, G.L. Wang, J. Power Sources 190 (2009) 346–350.
[4] G.H. Miley, N. Luo, J. Mather, R. Burton, G. Hawkins, L.F. Gu, E. Byrd, R. Gimlin, P.J. Shrestha, G. Benavides, J. Laystrom, D. Carroll, J. Power Sources 165 (2007) 509–516.
[5] C. Ponce de León, F.C. Walsh, A. Rose, J.B. Lakeman, D.J. Browning, R.W. Reeve, J. Power Sources 164 (2007) 441–448.
[6] H.J. Wu, C. Wang, Z.X. Liu, Z.Q. Mao, Int. J. Hydrogen Energy 35 (2010) 2648–2651.
[7] R.L. Pecsok, J. Am. Chem. Soc. 75 (1953) 2862–2864.
[8] J.H.H. Kim, S. Kim, Y.M. Kang, M.S. Song, S. Rajendran, S.C. Han, D.H. Jung, J.Y. Lee, J. Electrochem. Soc. 151 (2004) A1039–A1043.

[9] E. Gyenge, Electrochim. Acta 49 (2004) 965–978.
[10] D.A. Finkelstein, N.D. Mota, J.L. Cohen, H.D. Abruña, J. Phys. Chem. C 113 (2009) 19700–19712.
[11] M.V. Mirkin, H. Yang, A.J. Bard, J. Electrochem. Soc. 139 (1992) 2212–2217.
[12] V.W.S. Lam, E. Gyenge, J. Electrochem. Soc. 155 (2008) B1155–B1160.
[13] M.H. Atwan, D.O. Northwood, E.L. Gyenge, Int. J. Hydrogen Energy 30 (2005) 1323–1331.
[14] J.Q. Yang, B.H. Liu, S. Wu, J. Power Sources 194 (2009) 824–829.
[15] E. Sanli, H. Celikkan, B.Z. Uysal, M.L. Aksu, Int. J. Hydrogen Energy 31 (2006) 1920–1924.
[16] J. Ma, Y. Sahai, R.G. Buchheit, J. Power Sources 195 (2010) 4709–4713.
[17] D.M.F. Santos, C.A.C. Sequeira, J. Electrochem. Soc. 157 (2010) B13–B19.
[18] B.H. Liu, M. Chatenet, J. Alloys Compd. 454 (2008) 280–285.
[19] M. Chatenet, B. Molina-Concha, J.P. Diard, Electrochim. Acta 54 (2009) 1687–1693.
[20] M. Chatenet, F.H.B. Lima, E.A. Ticianelli, J. Electrochem. Soc. 157 (2010) B697–B704.
[21] H.C. Elikkana, M.S. Ahin, M.L. Aksu, T.N. Veziroglu, Int. J. Hydrogen Energy 32 (2007) 588–593.
[22] H. Cheng, K. Scott, Electrochim. Acta 51 (2006) 3429–3433.
[23] C. Ponce-de-león, D.V. Bavykin, F.C. Walsh, Electrochem. Commun. 8 (2006) 1655–1660.
[24] J.I. Martins, M.C. Nunes, R. Koch, L. Martins, M. Bazzaoui, Electrochim. Acta 52 (2007) 6443–6449.
[25] P. Hernández-Fernández, M. Montiel, P. Ocón, J.L.G. Fierro, H. Wang, H.D. Abruña, S. Rojas, J. Power Sources 195 (2010) 7959–7967.
[26] G.J. Wang, Y.Z. Gao, Z.B. Wang, C.Y. Du, J.J. Wang, G.P. Yin, J. Power Sources 195 (2010) 185–189.
[27] W.J. Zhou, S.Q. Song, W.Z. Li, Z.H. Zhou, G.Q. Sun, Q. Xin, S. Douvartzides, P. Tsiakaras, J. Power Sources 140 (2005) 50–58.
[28] V. Baglio, A.S. Aricò, A. Stassi, C.D. Urso, A.D. Blasi, A.M.C. Luna, V. Antonucci, J. Power Sources 159 (2006) 900–904.
[29] H. Yang, N. Alonso-Vante, J.M. Léger, C. Lamy, J. Phys. Chem. B 108 (2004) 1938–1947.
[30] G.J. Wang, Y.Z. Gao, A.B. Wang, C.Y. Du, J.J. Wang, G.P. Yin, J. Power Sources 195 (2010) 185–189.
[31] E. Gyenge, M. Atwan, D. Northwood, J. Electrochem. Soc. 153 (2006) A150–A158.
[32] P.Y. He, Y. Wang, X.Y. Wang, F. Pei, H. Wang, L. Liu, L.H. Yi, J. Power Sources 196 (2011) 1042–1047.
[33] J.J. Niu, J.N. Wang, Electrochim. Acta 53 (2008) 8058–8063.
[34] J.J. Wang, G.P. Yin, J. Zhang, Z.B. Wang, Y.Z. Gao, Electrochim. Acta 52 (2007) 7042–7050.
[35] A. Pozio, M.D. Francesco, A. Cemmi, F. Cardellini, L. Giorgi, J. Power Sources 105 (2002) 13–19.
[36] F. Maillard, M. Martin, F. Gloaguen, J.M. Léger, Electrochim. Acta 47 (2002) 3431–3440.
[37] R. Kou, Y.Y. Shao, D.H. Wang, M.H. Engelhard, J.H. Kwak, J. Wang, V.V. Viswanathan, C.M. Wang, Y.H. Lin, Y. Wang, I.A. Askay, J. Liu, Electrochem. Commun. 11 (2009) 954–957.
[38] J.J. Wang, G.P. Yin, Y.Y. Shao, S. Zhang, Z.B. Wang, Y.Z. Gao, J. Power Sources 171 (2007) 331–339.
[39] B.M. Concha, M. Chatenet, Electrochim. Acta 54 (2009) 6119–6129.
[40] H.H. Strehblow, V. Maurice, P. Marcus, Electrochim. Acta 46 (2001) 3755–3766.
[41] M.H. Atwan, C.L.B. Macdonald, D.O. Northwood, E. Gyenge, J. Power Sources 158 (2006) 36–44.
[42] C. Ponce-de-león, F.C. Walsh, C.J. Patrissi, M.G. Medeiros, P.R. Bessette, R.W. Reeve, J.B. Lakeman, A. Rose, D. Browening, Electrochem. Commun. 10 (2008) 1610–1613.